

Inverted Core/Shell Nanocrystals Continuously Tunable between Type-I and Type-II Localization Regimes

L. P. Balet, S. A. Ivanov, A. Piryatinski, M. Achermann, and V. I. Klimov*

Los Alamos National Laboratory, Los Alamos, New Mexico 87545

Received June 4, 2004

ABSTRACT

We study inverted core/shell nanocrystals (NCs) in which a core of a wide gap semiconductor (ZnSe) is overcoated with a shell of a semiconductor of a narrower gap (CdSe). By monitoring radiative recombination lifetimes for a series of these NCs with a fixed core radius and progressively increasing shell thickness, we observe a continuous transition from Type-I (both electron and hole wave functions are distributed over the entire NC) to Type-II (electron and hole are spatially separated between the shell and the core) and back to Type-I (both electron and hole primarily reside in the shell) localization regimes. These observations are in good agreement with the calculated dependence of the electron–hole overlap integral on shell thickness.

The use of multicomponent semiconductor heterostructures provides an interesting opportunity for designing electronic properties of materials via engineered spatial distributions of electron and hole wave functions.¹ In addition to a “trivial” control of confinement energies, such structures can allow one to control the dynamics of both single and multiexciton states by engineering the electron–hole (e–h) wave function overlap^{1–3} and the strength of Coulomb exciton–exciton interactions.^{4,5} Wave function engineering has been extensively explored using epitaxial quantum-well heterostructures.¹ In the case of semiconductor nanocrystals (NCs), the concept of combining different materials in a single nanoparticle has been mainly studied in the context of core/shell NCs, in which the shell material has a considerably wider gap than the material of the core.^{6–9} In this approach, the electron and hole experience a confinement potential that tends to localize both of the carriers in the NC core (Type-I localization), which reduces their interactions with surface trap states and improves the NC emission quantum yields. Core/shell NCs can also provide “spatially indirect” states, in which electrons and holes are spatially separated between the core and the shell (Type-II localization).^{2,3} Type-II CdSe/CdTe NCs have demonstrated emission at energies smaller than the band gap of either the core or the shell material as a result of spatially indirect transitions.³ Because of the reduced e–h wave function overlap, these structures show extended exciton lifetimes, useful, e.g., in photovoltaics and photocatalysis. Recently, it was also demonstrated that Type-II structures can show a regime of repulsive exciton–exciton interactions that can be used to considerably reduce the lasing thresholds for NCs in the green-blue range of emission colors.⁵

Here we report inverted ZnSe/CdSe hetero-NCs, in which a wide-gap semiconductor core is overcoated with a shell of a narrower gap material. We show that while CdSe and ZnSe are characterized by Type-I energy offsets in the bulk form, ZnSe/CdSe core/shell structures can exhibit either Type-I or Type-II behaviors, depending on the core radius and the shell thickness. To detect changes in carrier localization, we perform measurements of radiative lifetimes that provide direct information on the e–h overlap integral. Our studies of a series of NC samples with a fixed average core radius and progressively increasing shell thickness indicate that localization continuously changes from Type-I (electron and hole are delocalized over the entire NC) to Type-II (the electron is localized primarily in the shell while the hole wave function is still distributed over the entire NC, but with much greater probability in the core than in the shell) and then back to Type-I (both electron and hole are primarily localized in the shell).

In the case of bulk ZnSe/CdSe interfaces, the ZnSe valence-band edge is lower than that in CdSe (energy offset $U_0^h = 0.14$ eV), while the conduction-band edge is lower in CdSe ($U_0^c = 0.86$ eV) (Figure 1a). Such energy alignment nominally corresponds to the Type-I regime, in which both carriers (electron and hole) tend to be co-located in CdSe to produce an excitation with the lowest total energy. The situation, however, can change in the case of nanostructures, in which the alignment of quantized energy states is determined not only by bulk energy offsets but also confinement energies determined by the heterostructure dimensions.

To analyze the spatial distributions of electron and hole wave functions in inverted ZnSe/CdSe NCs as a function of the core radius (R_c) and the shell thickness (d), we apply the two-band, effective-mass approximation using a spherically

* Corresponding author. E-mail: klimov@lanl.gov.

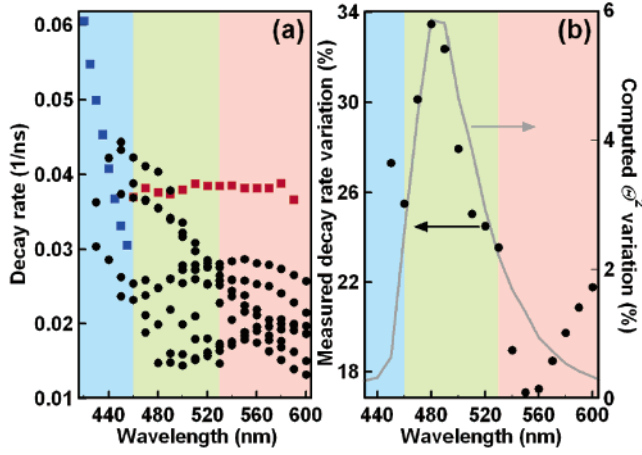


Figure 3. (a) Spectrally resolved radiative decay rates measured for inverted ZnSe/CdSe NCs (black circles) and monocomponent ZnSe (blue squares), and CdSe (red squares) NCs. (b) Standard deviation of decay rates measured for a given wavelength (black circles) in comparison to standard deviation of the calculated e–h overlap integral. Both sets of data show maximum in the range of Type-II localization.

wavelength lines. Two gray lines in this plot indicate the boundaries of the Type-II localization regime. For $R_c = 15$ Å, the emission wavelengths corresponding to this regime are approximately from 460 to 530 nm. One interesting observation is that a given emission wavelength cannot be uniquely related to a pair of the NC geometrical parameters R_c and d , because the same emission wavelengths can be produced by different combinations of R_c and d . Furthermore, the same emission wavelength can correspond to different localization regimes. To illustrate this point we calculate the e–h overall integral, $\Theta^2 = |\langle \psi^h | \psi^e \rangle|^2$, for different combinations of R_c and d and plot it in Figure 2b as a function of emission wavelength (different points at the same wavelength λ in Figure 2b correspond to different combinations of R_c and d that produce emission at λ). Spatial separation of an electron and a hole in the Type-II regime should produce a reduced overlap integral. The latter quantity can, therefore, be used to detect changes in the spatial distributions of the electron and hole wave functions. The plot in Figure 2b indicates quite strong variations in Θ^2 for a given wavelength, indicating a variety of confinement regimes that produce emission with the same spectral energy. The important observation, however, is that while the overlap integral itself cannot be uniquely related to a certain emission wavelength, its variation (calculated in terms of a standard deviation, $\delta\Theta^2$) is a “unique” function of λ (line in Figure 3b). Furthermore, $\delta\Theta^2$ shows a well-pronounced maximum in the wavelength range in which hetero-NCs exhibit the Type-II localization. On the basis of these considerations, in our experimental analysis below, we use the variation in the overlap integral as a probe of the localization regime.

In our experimental studies we use ZnSe/CdSe core/shell NCs fabricated via a controlled deposition of CdSe onto preformed ZnSe seed particles.⁵ The NCs are excited at 402 nm with 50 ps pulses from a pulsed diode laser at low pump intensities of $<0.5 \mu\text{J}/\text{cm}^2/\text{pulse}$. These pump levels correspond to the excitation of less than 0.01 e–h pairs per dot

per pulse on average, which allows us to neglect multiexciton effects. The NC photoluminescence (PL) is spectrally dispersed using a monochromator and detected with a cooled multichannel plate photomultiplier tube. When combined with a time-correlated single photon counting system, this setup provides a time resolution of 70 ps. In our studies we only use high (60–80%) PL quantum yield NCs, for which e–h recombination is dominated by radiative processes. Furthermore, to make sure that our results are not affected by fast surface/interface trapping processes, we derive time constants from the data toward the end of the decay, in the range of 50–140 ns. All measurements are performed at room temperature on solutions of ZnSe/CdSe NCs in hexane.

As an experimental measure of the e–h overlap integral, we use the rate of the radiative decay, Γ , which is directly proportional to Θ^2 (ref 10). In Figure 3a, we show the plot of the radiative decay rates vs emission wavelength derived from the PL dynamics of a series of core/shell samples with a fixed average core radius (15 Å) and several different shell thicknesses. Depending on the shell thickness, the emission wavelength of the NC samples varies from 430 to 600 nm. According to our theoretical modeling, this range spans all possible localization regimes, from the confinement of electron and hole primarily in the core to the confinement of both carriers in the shell. The relaxation data shown as circles in Figure 3a summarize the results obtained for different core/shell samples in the series. For each sample we derived several time constants for different wavelengths within the inhomogeneously broadened emission line. Because of the dispersion of both core and shell sizes in our samples, the emission at a given wavelength can be produced by NCs with different combinations of core and shell radii, which can correspond to different localization regimes. Thus, we obtain several different time constants for each measured wavelength. For comparison, in Figure 3a we also plot spectrally resolved relaxation rates measured for monocomponent ZnSe (blue squares) and CdSe (red squares) NCs.

The data set shown for CdSe NCs spans almost the same spectral range as that studied for core/shell structures. In this range, CdSe NCs do not show any significant dependence of decay rates on the emission wavelength, which is a result of nearly size-independent radiative lifetime in CdSe nanoparticles.¹¹ In contrast to this behavior, the hetero-NCs show strong spectral variations in decay rates. One trend is the reduction in the recombination rate in the range from ~ 430 nm to ~ 490 nm, consistent with the expected transition from Type-I (both carriers primarily in the core) to Type-II (carriers spatially separated between core and shell) localization. The rates observed on the blue end of this range (thin shells) are $\sim 0.04 \text{ ns}^{-1}$ (the respective recombination time is ~ 25 ns). This value is close to rates measured at the same spectral energies for purely ZnSe NCs (blue squares), confirming that in hetero-NCs with thin shells both electron and hole reside primarily in the core.

While some general trends associated with the effect of carrier localization on recombination dynamics can be seen in the plot in Figure 3a, the analysis of rate vs. wavelength data is significantly complicated by a wide spread of

relaxation rates observed for any given detection wavelength. As already mentioned, this spread results from both sample polydispersity and the intrinsic property of ZnSe/CdSe hetero-NCs to produce the same emission wavelengths for different combinations of R_c and d . However, as indicated by our theoretical modeling, the variation of relaxation rates can provide useful information on changes in the localization regime.

The transitions between different localization regimes indeed appear quite pronounced in spectrally resolved recombination-rate variation data measured in terms of the standard deviation, $\delta\Gamma$ (Figure 3b, circles). As expected from our theoretical modeling (line in Figure 3b), $\delta\Gamma$ shows a well-resolved maximum in the spectral range of Type-II localization. It falls off on both sides of this range following the calculated variation in the e–h overlap integral, indicating a transition to Type-I localization. From the spectral position and the width of the $\delta\Gamma$ peak (measured at a half-height), we estimate that Type-II localization occurs in the range of wavelengths from ~ 460 nm to ~ 530 nm, which is in remarkable agreement with the results of our calculations.

In conclusion, we have shown both theoretically and experimentally that ZnSe/CdSe core/shell NCs can exhibit both Type-I and Type-II behaviors, depending on core size and shell thickness. To detect the transition between different localization regimes, we used time- and spectrally resolved PL measurements, which provided direct information on the e–h overlap integral. We observed strong variations in decay rates measured at the same wavelength for hetero-NCs of different average dimensions. These variations relate to the fact that ZnSe/CdSe can produce the same emission wavelength for different combinations of the core radius and the shell thickness that can correspond to different localization

regimes (and hence different e–h overlap integrals). Further, we have demonstrated that the variation in relaxation rates exhibit a well defined maximum in the spectral range of Type-II localization. We applied the analysis of the variation in recombination rates to experimentally detect the transition between different localization regimes.

Acknowledgment. This work was supported by Los Alamos LDRD Funds and the Chemical Sciences, Biosciences, and Geosciences Division of the Office of Basic Energy Sciences, Office of Science, U.S. Department of Energy.

References

- (1) *Quantum heterostructures: microelectronics and optoelectronics*; Mitin, V. V., Kochelap, V. A., Stroschio, M. A., Eds.; Cambridge University Press: Cambridge, 1999.
- (2) Kortan, A. R.; Hull, R.; Opila, R. L.; Bawendi, M. G.; Steigerwald, M. L.; Carroll, P. J.; Brus, L. E. *J. Am. Chem. Soc.* **1990**, *112*, 1327, 1990.
- (3) Kim, S.; Fisher, B.; Eisler, H.-J.; Bawendi, M. *J. Am. Chem. Soc.* **2003**, *125*, 11466.
- (4) Butov, L. V.; Gossard, A. C.; Chemla, D. S. *Nature* **2002**, *418*, 751.
- (5) Ivanov, S. A.; Nanda, J.; Piryatinski, A.; Achermann, M.; Balet, L. P.; Bezel, I. V.; Anikeeva, P. O.; Tretiak, S.; Klimov, V. I. *J. Phys. Chem. B*, in press.
- (6) Peng, X.; Schlamp, M. C.; Kadavanich, A. V.; Alivisatos, A. P. *J. Am. Chem. Soc.* **1997**, *119*, 7019.
- (7) Hines, M. A.; Guyot-Sionnest, P. *J. Phys. Chem.* **1996**, *100*, 468.
- (8) Dabbousi, B. O.; Rodriguez-Viejo, J.; Mikulec, F. V.; Heine, J. R.; Mattoussi, H.; Ober, R.; Jensen, K. F.; Bawendi, M. G. *J. Phys. Chem. B* **1997**, *101*, 9463.
- (9) Cao, Y. W.; Banin, U. *Angew. Chem., Int. Ed.* **1999**, *38*, 3692.
- (10) Al. Efros, L. *Phys. Rev. B* **1992**, *46*, 7448.
- (11) Crooker, S. A.; Barrick, T.; Hollingsworth, J. A.; Klimov, V. I. *Appl. Phys. Lett.* **2003**, *82*, 2793.

NL049146C